Long Time-lapse Nanoscopy with Spontaneously Blinking Membrane Probes

Hideo Takakura[1,^], Yongdeng Zhang[1,^], Roman S. Erdmann[1,2,^], Alexander D. Thompson,[2,^] Yu Lin,[1] Brian McNellis[1], Felix Rivera-Molina[1], Shin-nosuke Uno[4], Mako Kamiya[3,5], Yasuteru Urano[3,4,6,], James E. Rothman[1], Joerg Bewersdorf[1,7], Alanna Schepartz[2,8*], Derek Toomre[1*]

[1]Department of Cell Biology, Yale University School of Medicine, 333 Cedar Street, New Haven, Connecticut, USA. [2]Department of Chemistry, 225 Prospect Street, Yale University, New Haven, Connecticut, USA. [3]Graduate School of Medicine and [4]Graduate School of Pharmaceutical Sciences, The University of Tokyo, 7-3-1 Hongo, Bunkyo-ku, 113-0033, Japan. [5]PRESTO, Japan Science and Technology Agency, 4-1-8 Honcho, Kawaguchi, Saitama, 332-0012, Japan. [6]CREST, Japan Agency for Medical Research and Development (AMED), 1-7-1 Otemachi, Chiyoda-ku, Tokyo, 100-0004, Japan. [7]Department of Biomedical Engineering, Yale University, 55 Prospect Street, New Haven, Connecticut, USA. [8]Department of Molecular, Cellular, and Developmental Biology, 216 Prospect Street, Yale University, New Haven, Connecticut, USA.

[^]Co-first authors, order determined by coin flip
[*]Corresponding authors, derek.toomre@yale.edu, alanna.schepartz@yale.edu

Abstract

Long time-lapse, diffraction-unlimited super-resolution imaging of cellular structures and organelles in living cells is highly challenging, as it requires dense labeling, bright, highly photostable dyes, and non-toxic conditions. We developed a set of high-density, environment-sensitive (HIDE) membrane probes based on HMSiR that assemble *in situ* and enable long time-lapse, live cell nanoscopy of discrete cellular structures and organelles with high spatio-temporal resolution. HIDE-enabled nanoscopy movies are up to 50x longer than movies obtained with labeled proteins, reveal the 2D dynamics of the mitochondria, plasma membrane, and filopodia, and the 2D and 3D dynamics of the endoplasmic reticulum in living cells. These new HIDE probes also facilitate the acquisition of live cell, two-color, super-resolution images, greatly expanding the utility of nanoscopy to visualize processes and structures in living cells.

Super-resolution fluorescence microscopes have dramatically surpassed the diffraction limit[1-4] and now allow the direct visualization of dynamic changes in cellular morphology at the nanoscale in living cells[4-12]. However, long time-lapse super-resolution imaging (nanoscopy) has been difficult to achieve, as it requires both high-density labeling[13, 14] and fluorophores with exceptional photostability[15, 16]. Most proteins, with the exception of protein polymers (*e.g.* tubulin, actin, clathrin), are not distributed at sufficiently high density to achieve dense labeling within the cell, and most small molecule and protein fluorophores are photo-inactivated within seconds under conditions required for SMS or STED experiments[9], which precludes image acquisition over long time scales.

Single molecule switching (SMS) nanoscopy (e.g. STORM[17], dSTORM[18], PALM[19], FPALM[20], GSDIM[21], etc.) further requires the precise localization of individual fluorescent molecules. SMS is typically achieved by driving fluorophores between OFF (dark) and ON (fluorescent) states using redox-active chemicals (for organic fluorophores) or light (for photo-convertible fluorescent proteins)[1, 2, 5, 7-9, 22]. However, using SMS nanoscopy to visualize intracellular components of live cells is challenging, because most organic SMS fluorophores are not membrane-permeable[7, 8, 23] and many that are permeant require toxic redox agents and oxygen depletion systems to increase their photostability. Although genetically encodable and photo-convertible fluorescent proteins such as mEos3.2[24] can facilitate intracellular SMS experiments without redox agents[19], photo-conversion requires activation with a potentially phototoxic 405 nm laser[25], and the photo-converted products possess limited photostability[15]. Moreover, experiments that exploit genetically encoded protein tags generally require transfection, and labeling density is limited inherently by protein expression. Further, two-color, live SMS nanoscopy cannot be achieved without an appropriate partner for mEos3.2. These interrelated experimental challenges make it virtually impossible to study dynamic cellular processes by nanoscopy for extended times, let alone in multicolor or in 3D.

Here we report that long time-lapse and two-color super-resolution imaging can be achieved with SMS nanoscopy using a series of high-density, environment-sensitive (HIDE) probes that localize the membrane permeable silicon-rhodamine dye HMSiR[26] at high density within a lipophilic membrane environment. Localization is achieved with a variety of *trans*-cyclooctene (TCO)-modified membrane probes that assemble *in cellulo* with HMSiR-Tz using bioorthogonal tetrazine chemistry[27] (**Supplementary Fig. 1a**). When localized to the membrane, HMSiR facilitates the acquisition of super-resolution movies in standard media (additive-free) up to 30 mins in length (more than 750 time points) without the need for UV activation. These movies reveal the 2D dynamics of the mitochondria, plasma membrane, and filopodia, as well as 2D and 3D dynamics of the endoplasmic reticulum in living cells.

These new HIDE probes also facilitate the acquisition of live cell, two-color, super-resolution images, greatly expanding the utility of nanoscopy to visualize processes and structures in living cells.

RESULTS

Hiding a Spontaneously Blinking High-Density Lipid Probe in a Dark State

The SMS dye HMSiR blinks spontaneously by virtue of a reversible intramolecular spirocyclization event that interconverts a closed and neutral dark form (OFF) with an open and charged fluorescent form (ON)[26] (**Fig. 1a**). The position of the HMSiR ON/OFF equilibrium is pH-dependent: in phosphate buffer (pH 7.4), the fraction of dye in the ON state is 1.2-1.3% (see Methods). However, even an ON fraction of 1.2-1.3% is too high for SMS nanoscopy in a densely labeled field: under these conditions many signals are rejected because the signals of single molecules partially overlap, and photobleaching of molecules in the ON state drains the population of photoactive molecules,precluding the acquisition of long time-lapse images. We reasoned that shifting the HMSiR ON/OFF ratio to ultra-low values could virtually eliminate both problems: Under these conditions, fewer single molecules would be rejected due to partial colocalization, allowing for increased effective labeling density, and fewer molecules would be simultaneously in the ON state, decreasing the drain of photoactive molecules and favoring the acquisition of long time-lapse images. Given that the HMSiR ON/OFF equilibrium interchanges a neutral, dark state with a fluorescent, charged state, we hypothesized that placing HMSiR in a hydrophobic environment, such as within a membrane, would shift the ON/OFF ratio to ultra-low values. We further hypothesized that combining an ultra-low ON/OFF ratio with high labeling density would improve both image quality and apparent photostability–the length of time during which images can be obtained.

Optimization of HMSiR blinking for Speed, Resolution, and Environment

As a prelude, to optimize the spatial and temporal resolution of SMS images obtained with HMSiR, we made use of an *in vitro* SMS assay and a fast sCMOS camera[9] to monitor the relationship between laser intensity and eight photophysical parameters (**Supplementary Fig. 2**). These experiments revealed an improved localization precision (from σ = 22 nm to ~12 nm) when the laser power was increased from 1.5 to ~4-10 kW/cm^2 (**Supplementary Fig. 2c**), effectively doubling the spatial resolution and improving the temporal resolution by 10-fold when compared with prior studies with HMSiR[16] (**Supplementary Fig. 3**). Next, using these parameters, we performed *in vitro* experiments to determine whether placing HMSiR in a hydrophobic environment would shift the ON/OFF ratio to ultra-low values and increase the apparent photostability. First, we synthesized HMSiR-tetrazine (HMSiR-Tz, **Supplementary Fig. 4**) and determined its absorbance in phosphate buffer containing increasing amounts

(10-70%) of 1,4-dioxane. As demonstrated with the related dye SiR-carboxyl[12], the absorbance of HMSiR at 653 nm (the absorbance maximum of the open, fluorescent form) was highest in solutions containing the smallest amount of dioxane (10%) (**Supplementary Fig. 5**); increasing the dioxane content led to a systematic decrease in absorbance at 653 nm and a concomitant increase in absorbance at 280 nm (the absorbance maximum of the closed, dark form). Next, to evaluate directly whether localization to a hydrophobic environment would improve the apparent photostability of HMSiR, we imaged HMSiR *in vitro* in both an aqueous and a lipid environment and compared the observed number of localizations as a function of time. HMSiR was localized within an aqueous environment by conjugating HMSiR-CA to a Halo-tagged protein (Halo-GST) immobilized on glass; HMSiR was localized within a lipid environment by conjugating HMSiR-Tz to liposomes containing ceramide-*trans*-cylooctene (Cer-TCO)[28] (**Fig. 1b and c**). Evaluation of the decrease in the number of localizations as a function of time revealed that the time-dependent signal loss of HMSiR in a lipid environment was >6-fold slower than in an aqueous environment (**Fig. 1d**). The ON fraction in both environments was estimated by fitting the number of localizations per frame as a function of time: these values were 0.20 ± 0.04% for GST-HMSiR (aqueous environment) and 0.033 ± 0.002% for Cer-HMSiR (liposomes), a 6-fold decrease (**Supplementary Table 1**). These observations support the hypothesis that localizing HMSiR to a hydrophobic environment, such as within a membrane, can shift the ON/OFF equilibrium towards the neutral, dark form, reduce the ON fraction, and prolong imaging time. Indeed, the benefits of "hiding" HMSiR in a membrane environment are also supported by Monte Carlo SMS simulations, which indicate that combining an ultra-low ON fraction (0.01%) with high density labeling can facilitate a >20-fold increase in the number of frames with detectable images when compared with a low ON fraction (1%) and with 50-fold lower labeling density (**Supplementary Fig. 6** and **Supplementary Movie 1**).

Long Time-lapse Imaging of the ER with the Spontaneously Blinking HIDE Probe Cer-HMSiR

Previous work has shown that the ceramide lipid Cer-TCO accumulates in the Golgi after a temperature block (20 °C) and undergoes rapid reaction with the STED dye SiR-Tz to form a conjugate Cer-SiR that is benign to exocytic trafficking[28]. Although the reaction product of Cer-TCO and HMSiR-Tz localizes to the Golgi (**Supplementary Fig. 7a**), the pH of the Golgi (6.4 ± 0.3)[29] is too low to shift the ON/OFF ratio of Cer-HMSiR to an ultra-low value. We hypothesized that in the absence of a temperature block, Cer-TCO would also localize to the ER, whose pH is higher (pH 7.2 ± 0.2)[29]. Indeed, at 37 °C, cells treated with Cer-TCO and HMSiR-Tz and imaged showed evidence of colocalization between Cer-HMSiR and the ER-marker[30] KDELR-mEos3.2 as well as the Golgi marker[31] GalNAc T2-GFP

(**Supplementary Fig. 7b**). Based on the extended imaging of HMSiR in liposomes (**Fig. 1d**) and Monte Carlo simulations (**Supplementary Fig. 6**), we predicted that reaction of HMSiR-Tz with Cer-TCO in live cells would generate the conjugate Cer-HMSiR and enable long time-lapse super-resolution imaging of the ER (**Fig. 2a**). Live-cell SMS imaging of the ER labeled *in vivo* with Cer-HMSiR revealed multiple tubules in the cell periphery that were ~50 ± 3 nm wide (**Fig. 2b**), a value comparable to ER morphology metrics determined using electron microscopy[32]. As shown in **Fig. 2b**, a cell labeled with Cer-HMSiR could be imaged for 500 s (8 min) with a temporal resolution of 2 s (250 images); during this time, individual tubules remained visible (**Fig. 2b**, kymograph; right panel) and new tubules were observed (**Fig. 2b**, yellow arrowheads). A 2 s SMS snapshot from a 25 min time-lapse movie of another cell (**Fig. 2c**, see **Supplementary Movie 2**) clearly distinguished ER tubules (t) and sheets (s). Remarkably, over the course of 25 min, small buds appeared within dense tubules, and individual tubules extended, reversed, and formed small loops (arrowheads) (**Fig. 2d**, **Supplementary Fig. 8, Supplementary Movie 3**). ER structures also dynamically interconverted between tubules and sheets (**Fig. 2e** and **2f**, arrowheads). The temporal resolution can be increased to up to 0.1 s, but image quality suffers (**Supplementary Fig. 9** and **Supplementary Movie 4**). Direct comparison between long time-lapse SMS and diffraction-limited images indicate that nanoscale dynamics were evident only at super-resolution (**Supplementary Movie 5**). Cells labeled with Cer-HMSiR can be imaged for tens of minutes whereas those labeled with ER-tracker Red^{TM} bleach within two minutes, and additionally ER-tracker Red^{TM} requires photoactivation as well as a potentially cytotoxic oxygen depletion system for imaging (**Supplementary Fig. 10**). To the best of our knowledge **Supplementary Movie 2** is the longest movie ever recorded with a lateral spatial resolution < 50 nm and a 2 s temporal resolution. Moreover, illumination with far-red excitation (642 nm)– a key feature of the silicon-rhodamine scaffold–is far less phototoxic than excitation in the UV to visible spectrum[25]: even after 15 min of SMS illumination, 60% of the imaged HeLa cells remained viable (**Supplementary Fig. 11**).

These results indicate that long time-lapse super-resolution imaging (>20 min) of ER dynamics can be achieved when the labeling density is high and the ON/OFF ratio of HMSiR is shifted to ultra-low values within a hydrophobic membrane environment. The advantages of this combination are most evident by comparing the images obtained when HMSiR is conjugated to an ER-resident protein[33], such as Halo-Sec61β[11], or to the lipid probe Cer-TCO (**Supplementary Movie 6**). Although the signal from Sec61β-HMSiR was initially 2.3-fold higher than that from Cer-HMSiR, it decayed far more rapidly (**Fig. 2g**). An exponential fitting of the number of localizations as a function of time revealed that the signal from Sec61β-HMSiR decayed with a lifetime of τ = 7.6 ± 0.8 s, in good agreement with the value

determined *in vitro* (τ = 7.6 ± 0.5; **Fig. 1d**) whereas the signal from Cer-HMSiR decayed with a lifetime of τ = 414 ± 27 s, a 55-fold increase (**Fig. 2h**). A more detailed analysis of the imaging data revealed that the labeling density provided by Sec61β-HMSiR was 163 ± 17 molecules/μm^2 whereas the density provided by Cer-HMSiR was 5040 ± 1253 molecules/μm^2, a 31-fold increase (**Supplementary Table 1**). The ON fraction in both cases was estimated by fitting the number of localizations per frame as a function of time: these values were 0.178 ± 0.036% for Sec61β-HMSiR and 0.0024 ± 0.0006% for Cer-HMSiR, a 52-fold decrease (**Supplementary Table 1**). These quantitative comparisons reveal that combining a 30-fold higher labeling density with a 50-fold lower ON ratio enables the acquisition of SMS images over 750 frames, fully in line with the qualitative predictions of the Monte Carlo simulation.

To extend these findings, we next asked whether the combined benefits of an ultra-low ON fraction and high labeling density would enable super-resolution imaging of other cellular organelles. Although biochemical and lipidomic studies[34] have provided detailed information about organelle-specific lipid distributions, we hypothesized that a simpler approach would exploit established organelle-specific membrane dyes, suitably modified with an appended TCO to enable *in situ* conjugation with HMSiR-Tz, to enable super-resolution imaging of both the mitochondria and plasma membrane.

Long Time-lapse Nanoscopy Imaging of Mitochondria with the HIDE Probe RhoB-HMSiR

Cationic rhodamine derivatives localize to mitochondria[35], but do not blink spontaneously[8]. We synthesized the cationic rhodamine derivative RhoB-TCO (**Fig. 3a**) in two steps from commercially available Rhodamine B (**Supplementary Fig. 12**). Cells treated with RhoB-TCO and HMSiR-Tz showed evidence of colocalization between RhoB-HMSiR and the mitochondrial marker[36] tdEos-TOM20 (**Supplementary Fig. 13**). When imaged under SMS conditions, the mitochondria[37] of cells expressing Halo-OMP25 and treated with HMSiR-CA to generate OMP25-HMSiR could be visualized for only 20 s (**Fig. 3b**, kymograph; right panel) whereas those of cells treated with RhoB-TCO and HMSiR-Tz to generate RhoB-HMSiR could be imaged for more than 400 s (7 min) with a temporal resolution of 2 s (**Fig. 3c**, **Supplementary Movie 7**). Individual mitochondria remained visible throughout the entire movie (**Fig. 3c**, kymograph). The SMS images also revealed a branching mitochondrial network that is blurred in the diffraction-limited image **(Fig. 3d).** An exponential fitting of the number of localizations over time showed that the signal from RhoB-HMSiR decayed with a lifetime of τ = 196 ± 57 s while the signal from TOM20-HMSiR decayed 13-fold faster (τ = 15 ± 2.9 s) (**Supplementary Table 1**). A more detailed analysis of the imaging data revealed that RhoB-HMSiR provided a labeling density of 1014 ± 198 molecules/μm^2, whereas the

density was 400 ± 100 molecules/μm^2 with OMP25-HMSiR. The ON fraction in both cases was estimated as described above; these values were calculated as 0.0044 ± 0.0011% and 0.062 ± 0.018%, respectively (**Supplementary Table 1**). The 15-fold lower ON fraction of RhoB-HMSiR when compared with OMP25-HMSiR correlates well with the 20-fold increase in the number of acquired images, providing a second example in which hiding HMSiR in a membrane environment at high density provides tangible benefits for long time-lapse super-resolution imaging.

Long Time-lapse Nanoscopy Imaging of Plasma Membrane Dynamics with the HIDE Probe DiI-HMSiR

Another family of established organelle-specific dyes includes the dialkylindocarbocyanine DiI, which localizes to the plasma membrane[38]. Like RhoB, DiI does not blink spontaneously under physiological conditions.[8] We synthesized DiI-TCO (**Fig. 4a**) in one step from the previously reported[39] DiI-NH_2 (**Supplementary Fig. 14**). Cells treated with DiI-TCO and HMSiR-Tz and imaged showed evidence of colocalization between DiI-HMSiR and the plasma membrane marker[40] sspH-mSmo[41] (**Supplementary Fig. 15**). Super-resolution images of cells treated with DiI-TCO and HMSiR-Tz to form DiI-HMSiR *in situ* revealed the plasma membrane in great detail (**Fig. 4b**). Only in the SMS image are individual filopodia clearly distinguished from neighbors located as close as 160 nm apart and are resolved with a FWHM as low as 36 nm (**Fig. 4c**). Furthermore, the high resolution image also allowed visualization of the dynamic movement, growth, and retraction of filopodia (**Fig. 4d**, **Supplementary Movie 8**). An exponential fitting of the number of localizations over time showed that the signal from DiI-HMSiR decayed with a lifetime of τ = 171 ± 86 s while the signal from Smo-HMSiR decayed 14-fold faster (τ = 12 ± 6 s) (**Fig. 4g**). A more detailed analysis of the imaging data revealed that DiI-HMSiR provided a labeling density of 3220 ± 1458 molecules/μm^2, whereas the density was 435 ± 103 molecules/μm^2 with Smo-HMSiR, with ON fractions calculated as 0.011 ± 0.005% and 0.105 ± 0. 049%, respectively (**Supplementary Table 1**). Thus, in three different cases, combining high density labeling with the ultra-low ON fraction of HMSiR in a membrane environment facilitates long time-lapse super-resolution imaging of organelle dynamics. We predict that this strategy could be extended to more acidic organelles (endosomes and Golgi) using HMSiR variants whose spirocyclization equilibria are shifted towards the dark form at lower pH (lower pK_{cycle}).

The ON fraction of a HIDE Probe can be Reduced Further by Rational Design

Having validated the hypothesis that placing the spontaneously blinking dye HMSiR in a hydrophobic membrane environment at high density provides tangible benefits for SMS imaging, we next asked whether these benefits could be further enhanced by rational

changes in probe structure that further decrease the ON/OFF ratio. DiI derivatives localize within the plasma membrane with the aromatic chromophore oriented perpendicular to the bilayer plane[42]. We predicted that an analog of DiI-HMSiR containing a longer alkyl chain between the aromatic chromophore and the reactive TCO moiety (DiI-C6-TCO, **Fig. 4b**), would allow the appended HMSiR to more easily sample the hydrophobic bilayer interior, further shifting the ON/OFF equilibrium to the neutral, dark form. To test this hypothesis, we synthesized DiI-C6-TCO in one step from DiI-NH$_2$ (**Supplementary Fig. 14**). Cells treated with DiI-C6-TCO and HMSiR-Tz and imaged showed evidence of colocalization between DiI-HMSiR and the plasma membrane marker[40] sspH-mSmo[41] (**Supplementary Fig. 15**). Although in initial frames, the SMS super-resolution images of cells stained with DiI-C6-HMSiR were characterized by 23% fewer localizations than those stained by DiI-HMSiR, the signal from DiI-C6-HMSiR decayed significantly more slowly (**Fig. 4f**, **Supplementary Fig. 16**, **Supplementary Movie 9**). An exponential fitting of the number of localizations over time showed that the signal from DiI-HMSiR decayed with a lifetime of τ = 171 ± 86 s while the signal from DiI-C6-HMSiR decayed 2.4-fold more slowly with τ = 406 ± 72 s (**Fig. 4g**). Analysis of the imaging data revealed a labeling density of 3220 ± 1458 molecules/µm^2 and 4821 ± 1049 molecules/µm^2 for DiI-HMSiR and DiI-C6-HMSiR, respectively, with estimated ON fractions of 0.011 ± 0.005% and 0.0041 ± 0.0022% (**Supplementary Table 1**). Direct comparison of the apparent photostability of DiI-HMSiR and DiI-C6-HMSiR demonstrates the benefits of further decreases in the ON/OFF equilibrium of HMSiR achieved by rational design, with significant benefits for super-resolution SMS imaging of the boundaries of cellular organelles. Together, these additional examples of mitochondria and plasma membrane/filopodia imaging emphasize the general applicability of HIDE probes. Simultaneously increasing labeling density and decreasing ON/OFF ratio facilitates SMS imaging of membrane structures with high spatial and temporal resolution and over a previously unachievable timespan. One could easily imagine exploiting other organelle-specific lipids[34] or dyes[38] to image multiple discrete cellular compartments in this way.

2-Color Live Cell SMS Nanoscopy with HMSiR

Having established HMSiR as an excellent live-cell SMS dye, we posited that its photophysical properties should nicely complement those of the photoconvertible fluorescent protein mEos3.2[13]. We observed minimal crosstalk (<0.1%) when imaging HMSiR and mEos3.2 despite the wide emission band of the latter (**Supplementary Fig. 17).** To evaluate the suitability of HMSiR and mEos3.2 in two-color live-cell SMS nanoscopy, we tested whether the pair could effectively image various combinations of five different cellular targets/tags **(Fig. 5 b-d**, **Supplementary Fig. 18**). As expected, the proteins Sec61β[33] and

KDELR[30], when tagged with HMSiR and mEos3.2, respectively, localized extensively to the ER (**Fig. 5a**). Cross-sectional line profiles from both channels exhibit FWHM values of 53 ± 6 nm and 63 ± 12 nm for tubules labeled with Sec61β-HMSiR and KDELR-mEos3.2, respectively (**Fig. 5b**). Additionally, an axial line profile along a single tubule reveals the differential enrichment of Sec61β-HMSiR and KDELR-mEos3.2 in different regions of the tubule. In contrast, COPβ1-mEos3.2 often appeared in punctae that were distinct from HMSiR-tagged mitochondria (Halo-OMP25 + HMSiR-CA, **Fig. 5c**) and Golgi domains demarked by Cer-HMSiR (**Fig. 5d,e**). These proof-of-concept tests validate the use of HMSiR and mEos3.2 for dual-color live cell SMS imaging of intracellular targets.

Extending Live Cell HIDE Time-lapse Nanoscopy to 3D

Labeling density becomes even more essential to achieve high quality super-resolution images in three dimensions. To evaluate the benefits of Cer-HMSiR for long time-lapse 3D imaging of the ER, we visualized HeLa cells treated with Cer-TCO and HMSiR-Tz using a custom built 3D-SMS microscope. Images taken at the cell periphery reveal the ER as a clear three-dimensional network of tubules (**Fig. 6a** and **b**, **Supplementary Fig. 19**). Close-up views of the boxed volume in **Fig. 6b** when viewed from the top (along the z-axis, **Fig. 6c**) or from the side (along the y-axis, **Fig. 6d**) and represented as a 3D cartoon (**Fig. 6e**) reveal a level of network complexity that would be missed or misinterpreted when imaged in only two dimensions. For example, when imaged in 2D, the relative orientation of the four tubules t_1-t_4 in **Fig. 6c** would be ambiguous as they could represent either independent tubules or junctions. Only the 3D data reveals their true connectivity (**Fig. 6c-e**, **Supplementary Movie 10**). Tubules t_1 and t_4 are located in two different layers connected by a vertical sheet structure s_1 as seen on the left of **Fig. 6d** and on the left of **Fig. 6e**. There is a small gap between the tubules on the top layer (t_1 and t_2), which is indicated by the brown arrow (**Fig. 6c-e**). In addition, the relative orientation of tubules t_2 and t_3 can only be unambiguously determined by 3D imaging. They are located in two different layers, 560 nm apart (**Fig. 6d and Supplementary Fig. 20**), and only the 3D imaging reveals that they are connected by the vertical tubules c_1 and c_2 to form a loop like structure (**Fig. 6d and e**). We were able to image the cell shown in **Fig. 6a** for over 15 min with a temporal resolution of 10 s; the temporal resolution is, as expected, lower than in 2D due to the increased number of localizations needed to reconstruct a high-quality 3D image. This movie represents the longest live-cell movie achieved to date at such a high 3D resolution (**Supplementary Movie 11**, **Supplementary Movie 12** to be viewed with red/cyan 3D glasses). HMSiR in combination with Cer-TCO also facilitated the observation of 3D ER dynamics. Over the course of 266 s we could visualize a tubule elongating between different z-layers to form a junction on a lower layer before continuing to elongate and finally connecting with a third

tubule on a higher layer (**Fig. 6f**, red arrow heads, **Supplementary Movie 13**).

Finally, imaging closer to the cell center revealed not only the cytosolic ER, but also evidence that the ER traverses the nucleus (**Fig. 6g**). The 3D image in the x,y plane (**Fig. 6g**) and the y,z-cross section shown in **Fig. 6h** clearly show long, branching ER-derived channels within the nucleus[43]. The channel identified by the brown box exhibits a FWHM of 167 nm, whereas the ER structures associated with the nucleus exhibit a FWHM of 118 nm (**Fig. 6i**). The FWHM measured for the channel is consistent with values obtained from EM sections[43]. Notably, by use of HMSiR in combination with Cer-TCO, the axial FWHM of ER channels in the nucleus was improved 2-fold when compared to images of these invaginations obtained in fixed cells with immunostained lamin B by SIM[44]. These examples demonstrate the extraordinary versatility of the HMSiR/Cer-TCO combination for long time-lapse imaging of membrane structures and dynamics in three-dimensions. Many of these structures and dynamics would be invisible when imaged in two dimensions.

In summary, the HIDE probes and applications described herein greatly extend the utility of HMSiR for cellular imaging. Using diverse lipid probes that effectively "hide" the fluorophore within a membrane at high density, we achieved 2- and 10-fold increases in spatial and temporal resolution, respectively, 2-color imaging with mEos3.2, and 2D as well as 3D HIDE imaging of cellular dynamics of multiple membrane structures for tens of minutes. The importance of studying the structure and dynamics of the ER using super-resolution microscopy was recently highlighted by Nixon-Abell *et al.*[45]. The HIDE probe Cer-HMSiR represents a valuable tool for this purpose as it enables live cell (vs. fixed) imaging at a spatial resolution of 50 nm (vs. ~100 nm) in 2D as well as 3D live-cell imaging over 15 mins. Long time-lapse imaging with two-component HIDE probes is facile and versatile – it requires neither cell permeabilization, oxygen depletion, nor pre-bleaching, and easily accommodates multiple targets. HIDE probes greatly extend the imaging landscape for nanoscopy imaging of organelle dynamics. Future work will benefit from new HIDE probes that span the spectrum with orthogonal chemistries to enable nanoscopy analysis of multiple organelles over long times.

METHODS
Methods and any associated references are available in the online version of the paper.

AUTHOR CONTRIBUTIONS

H.T., Y.Z., R.S.E., A.D.T., J.B., A.S., J.E.R. and D.T. designed experiments. H.T., Y.Z., R.S.E., A.D.T., F.R.M., and Y.L. performed the imaging experiments. A.D.T designed and synthesized RhoB-TCO, DiI-TCO, and DiI-(C6-)TCO. R.S.E synthesized Cer-TCO. B.M. performed computer simulations. F.R.M. generated the COPβ1-mEos3.2 stable HeLa cell line. S.U., M.K. and Y.U. developed and synthesized HMSiR-Tz. H.T., R.S.E., A.D.T., J.B., A.S., and D.T. wrote the manuscript.

J.B. discloses significant financial interest in Bruker Corp. and Hamamatsu Photonics. R.S.E., A.D.T, D.T., and A.S. disclose a pending patent for novel lipid probes.

REFERENCES

1.   Hell, S.W. Far-field optical nanoscopy. *Science* **316**, 1153-1158 (2007).

2.   Huang, B., Babcock, H. & Zhuang, X.W. Breaking the Diffraction Barrier: Super-Resolution Imaging of Cells. *Cell* **143**, 1047-1058 (2010).

3.   Sahl, S.J. & Moerner, W.E. Super-resolution fluorescence imaging with single molecules. *Curr Opin Struc Biol* **23**, 778-787 (2013).

4.   Liu, Z., Lavis, L.D. & Betzig, E. Imaging Live-Cell Dynamics and Structure at the Single-Molecule Level. *Mol Cell* **58**, 644-659 (2015).

5.   Hess, S.T. et al. Dynamic clustered distribution of hemagglutinin resolved at 40 nm in living cell membranes discriminates between raft theories. *P Natl Acad Sci USA* **104**, 17370-17375 (2007).

6.   Manley, S. et al. High-density mapping of single-molecule trajectories with photoactivated localization microscopy. *Nat Methods* **5**, 155-157 (2008).

7.   Jones, S.A., Shim, S.H., He, J. & Zhuang, X.W. Fast, three-dimensional super-resolution imaging of live cells. *Nat Methods* **8**, 499-505 (2011).

8.   Shim, S.H. et al. Super-resolution fluorescence imaging of organelles in live cells with photoswitchable membrane probes. *P Natl Acad Sci USA* **109**, 13978-13983 (2012).

9.   Huang, F. et al. Video-rate nanoscopy using sCMOS camera-specific single-molecule localization algorithms. *Nat Methods* **10**, 653-658 (2013).

10.   Lukinavicius, G. et al. Fluorogenic probes for live-cell imaging of the cytoskeleton. *Nat Methods* **11**, 731-733 (2014).

11.   Bottanelli, F. et al. Two-colour live-cell nanoscale imaging of intracellular targets. *Nat Commun* **7** (2016).

12.   Lukinavicius, G. et al. A near-infrared fluorophore for live-cell super-resolution microscopy of cellular proteins. *Nat Chem* **5**, 132-139 (2013).

13.   Jungmann, R. et al. Multiplexed 3D cellular super-resolution imaging with DNA-PAINT and Exchange-PAINT. *Nat Methods* **11**, 313-318 (2014).

14.   Kiuchi, T., Higuchi, M., Takamura, A., Maruoka, M. & Watanabe, N. Multitarget super-resolution microscopy with high-density labeling by exchangeable probes (vol 12, pg 743, 2015). *Nat Methods* **12**, 893-893 (2015).

15.   Fernandez-Suarez, M. & Ting, A.Y. Fluorescent probes for super-resolution imaging in living cells. *Nat Rev Mol Cell Bio* **9**, 929-943 (2008).

16.   Toomre, D. & Bewersdorf, J. A New Wave of Cellular Imaging. *Annu Rev Cell Dev Bi* **26**, 285-314 (2010).

17.   Rust, M.J., Bates, M. & Zhuang, X.W. Sub-diffraction-limit imaging by stochastic optical reconstruction microscopy (STORM). *Nat Methods* **3**, 793-795 (2006).

18.   Heilemann, M. et al. Subdiffraction-resolution fluorescence imaging with conventional fluorescent probes. *Angew Chem Int Edit* **47**, 6172-6176 (2008).

19.   Betzig, E. et al. Imaging intracellular fluorescent proteins at nanometer resolution. *Science* **313**, 1642-1645 (2006).

20.   Hess, S.T., Girirajan, T.P.K. & Mason, M.D. Ultra-high resolution imaging by fluorescence photoactivation localization microscopy. *Biophys J* **91**, 4258-4272 (2006).

21.   Hell, S.W. & Kroug, M. Ground-State-Depletion Fluorescence Microscopy - a Concept for Breaking the Diffraction Resolution Limit. *Appl Phys B-Lasers O* **60**, 495-497 (1995).

22.   Shcherbakova, D.M., Sengupta, P., Lippincott-Schwartz, J. & Verkhusha, V.V. Photocontrollable Fluorescent Proteins for Superresolution Imaging. *Annu Rev Biophys* **43**, 303-329 (2014).

23.   Dempsey, G.T., Vaughan, J.C., Chen, K.H., Bates, M. & Zhuang, X.W. Evaluation of fluorophores for optimal performance in localization-based super-resolution imaging. *Nat Methods* **8**, 1027-1036 (2011).

24.   Zhang, M.S. et al. Rational design of true monomeric and bright photoactivatable fluorescent proteins. *Nat Methods* **9**, 727-729 (2012).

25. Waldchen, S., Lehmann, J., Klein, T., van de Linde, S. & Sauer, M. Light-induced cell damage in live-cell super-resolution microscopy. *Sci Rep-Uk* **5** (2015).

26. Uno, S.N. et al. A spontaneously blinking fluorophore based on intramolecular spirocyclization for live-cell super-resolution imaging. *Nat Chem* **6**, 681-689 (2014).

27. Devaraj, N.K., Hilderbrand, S., Upadhyay, R., Mazitschek, R. & Weissleder, R. Bioorthogonal Turn-On Probes for Imaging Small Molecules inside Living Cells. *Angew Chem Int Edit* **49**, 2869-2872 (2010).

28. Erdmann, R.S. et al. Super-Resolution Imaging of the Golgi in Live Cells with a Bioorthogonal Ceramide Probe. *Angew Chem Int Edit* **53**, 10242-10246 (2014).

29. Wu, M.M. et al. Organelle pH studies using targeted avidin and fluorescein-biotin. *Chem Biol* **7**, 197-209 (2000).

30. Munro, S. & Pelham, H.R.B. A C-Terminal Signal Prevents Secretion of Luminal Er Proteins. *Cell* **48**, 899-907 (1987).

31. Storrie, B. et al. Recycling of Golgi-resident glycosyltransferases through the ER reveals a novel pathway and provides an explanation for nocodazole-induced Golgi scattering. *J Cell Biol* **143**, 1505-1521 (1998).

32. Puhka, M., Joensuu, M., Vihinen, H., Belevich, I. & Jokitalo, E. Progressive sheet-to-tubule transformation is a general mechanism for endoplasmic reticulum partitioning in dividing mammalian cells. *Mol Biol Cell* **23**, 2424-2432 (2012).

33. Greenfield, J.J.A. & High, S. The Sec61 complex is located in both the ER and the ER-Golgi intermediate compartment. *J Cell Sci* **112**, 1477-1486 (1999).

34. van Meer, G., Voelker, D.R. & Feigenson, G.W. Membrane lipids: where they are and how they behave. *Nat Rev Mol Cell Bio* **9**, 112-124 (2008).

35. Ishigaki, M. et al. STED super-resolution imaging of mitochondria labeled with TMRM in living cells. *Mitochondrion* **28**, 79-87 (2016).

36. Yano, M. et al. Visualization of mitochondrial protein import in cultured mammalian cells with green fluorescent protein and effects of overexpression of the human import receptor Tom20. *J Biol Chem* **272**, 8459-8465 (1997).

37. Nemoto, Y. & De Camilli, P. Recruitment of an alternatively spliced form of synaptojanin 2 to mitochondria by the interaction with the PDZ domain of a mitochondrial outer membrane protein. *Embo J* **18**, 2991-3006 (1999).

38. Haugland Molecular Probes Handbook.

39. Leung, W.Y.H., R. P.; Mao, F. Lipophilic cyanine dyes with enhanced aqueous solubility.US6004536A   (1999).

40. Stone, D.M. et al. The tumour-suppressor gene patched encodes a candidate receptor for Sonic hedgehog. *Nature* **384**, 129-134 (1996).

41. Kukic, I., Rivera-Molina, F. & Toomre, D. The IN/OUT assay: a new tool to study

ciliogenesis. *Cilia* **5**, 23 (2016).

42.   Axelrod, D. Carbocyanine Dye Orientation in Red-Cell Membrane Studied by Microscopic Fluorescence Polarization. *Biophys J* **26**, 557-573 (1979).

43.   Fricker, M., Hollinshead, M., White, N. & Vaux, D. Interphase nuclei of many mammalian cell types contain deep, dynamic, tubular membrane-bound invaginations of the nuclear envelope. *J Cell Biol* **136**, 531-544 (1997).

44.   Schermelleh, L. et al. Subdiffraction multicolor imaging of the nuclear periphery with 3D structured illumination microscopy. *Science* **320**, 1332-1336 (2008).

45.   Nixon-Abell, J. et al. Increased spatiotemporal resolution reveals highly dynamic dense tubular matrices in the peripheral ER. *Science* **354** (2016).

Figure legends

Figure 1 Development of a high-density, environment-sensitive (HIDE) probe based on spontaneously blinking HMSiR for long time-lapse and 3D super-resolution imaging in living cells. (**a**) HMSiR dyes equilibrate between two forms, a closed, intramolecularly cyclized form, which is not emissive, and an open, uncyclized form that is fluorescent. The position of the HMSiR cyclization equilibrium depends on both pH and the polarity of the environment. (**b**) Cartoon of an *in vitro* experiment to assess whether the HMSiR ON/OFF fraction is affected by environment polarity. HMSiR was immobilized to a glass surface *via* either a protein (upon reaction of HMSiR-CA (**Supplementary Fig. 1b**) with Halo-GST) or a liposome (upon reaction of HMSiR-Tz (**Supplementary Fig. 1b**) with Cer-TCO[28]). (**c**) Super-resolution images of HMSiR immobilized as described in (**b**). Rainbow colored temporal look-up table. Scale bar: 200 nm. Laser intensity: 17.6 kW/cm^2. (**d**) Plot illustrating the normalized number of localizations observed as a function of time when HMSiR was immobilized to a protein, within an aqueous environment, and within a liposome, a hydrophobic environment. τ values were calculated from a single exponential fit (mean ± standard deviation (SD) of data from 9 fields of view (protein) or 40 individual liposomes.

Figure 2 Long time-lapse, wide-field SMS imaging of endoplasmic reticulum (ER) dynamics using the HIDE probe Cer-HMSiR generated upon reaction of Cer-TCO and HMSiR-Tz. (**a**) Schematic illustration of the 2-step procedure employed to label the ER with Cer-HMSiR. (**b**) Super-resolution image of the ER in HeLa cells showing time-colored localizations. A plot of the average fluorescent signal as a function of position along the 4 profiles shown as yellow lines is shown as an insert. The solid yellow line shows the signal in the super-resolution image, while the white dashed line shows the signal in the diffraction-limited image. These profiles are characterized by FWHM values (mean ± SD, n = 4) of 50 ± 3 nm (super-resolution image) and 367 ± 38 nm (diffraction-limited image). The elongation of an ER tubule later in the recording is indicated by a green arrow (top right corner). A kymograph (signal along the purple line profile as a function of time) is shown in the right side panel. The time-dependent appearance of new ER tubules is indicated by yellow arrowheads. Laser intensity: 9.9 kW/cm^2. Scale bar: 1 μm. (**c-f**) Super-resolution imaging of the ER in a live HeLa cell over 25 min. (**c**) One snap shot (t = 258 s) from a 25-min movie. The image was reconstructed from 800 frames recorded over 2 s and Kalman-filtered. *s*: sheet-like ER, *t*: tubular ER. Laser intensity: 9.9 kW/cm^2. Scale bar: 1 μm. The full 25 min movie is available as **Supplementary Movie 2.**   (**d**, **e**) Time-lapse images of ER dynamics. Each image was reconstructed from 800 frames, recorded over 2 s and Kalman-filtered. The full movie (1296 s) is available as **Supplementary Movie 3.** (**d**) Small ER regions are observed to bud off (yellow arrowhead), loop back (green arrowhead), and fuse (magenta and blue arrowheads). (**e**) ER sheets can reversibly transition into tube-like structures (white

arrowheads). Scale bar: 500 nm. (**f**) Kymograph (line profile versus time) of the purple line in (c). (**g**) Comparison of the number of localizations per μm^2 observed between HMSiR localized to a lipid (*via* Cer-HMSiR) and to a protein (*via* Sec61β-HMSiR) that resides within the ER. (**h**) τ values calculated from a single exponential fit to the photobleaching curves in **g** (mean ± SD, n = 3).
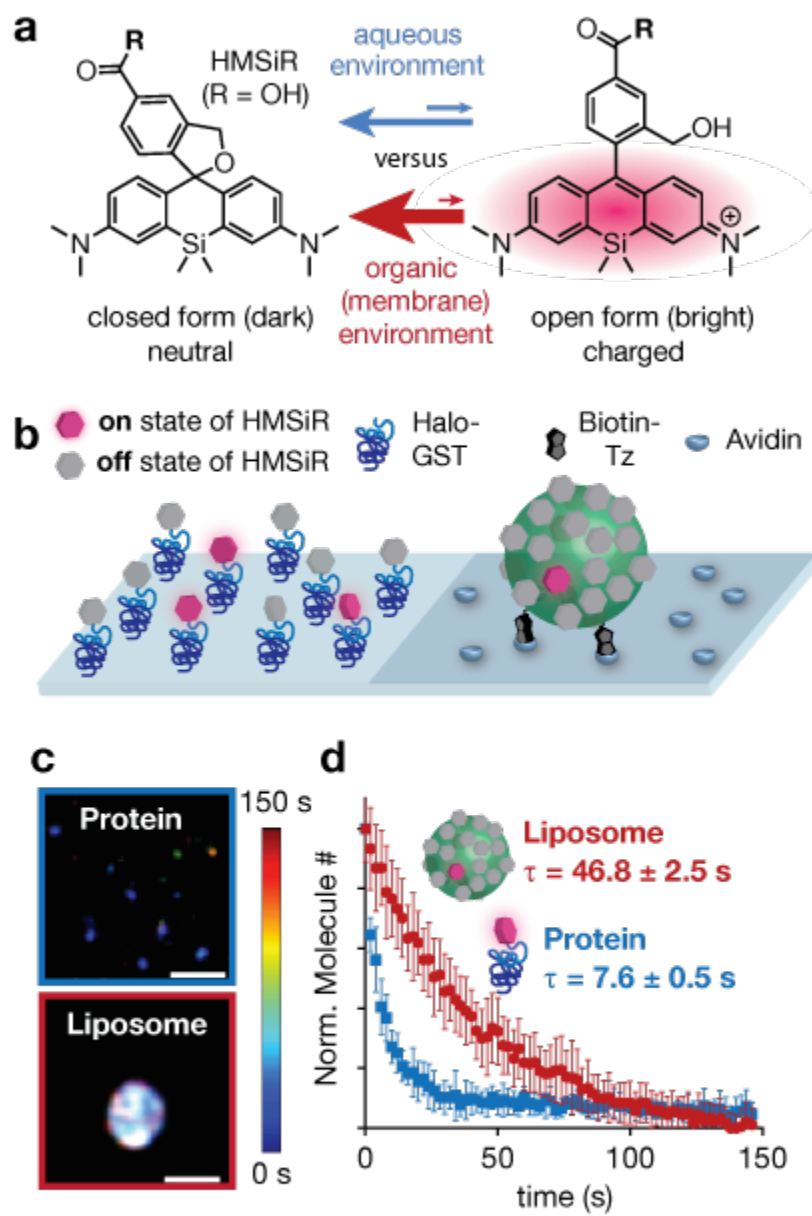
Figure 3 Long time-lapse, wide-field SMS imaging of mitochondria using the HIDE probe RhoB-HMSiR generated upon reaction of RhoB-TCO and HMSiR-Tz. (**a**) Chemical structure of RhoB-TCO and schematic illustration of the 2-step procedure employed to label mitochondria with RhoB-HMSiR. (**b,c**) Comparison between time-colored super-resolution images of mitochondria labeled with the protein probe Halo-OMP25-HMSiR and the HIDE probe RhoB-HMSiR. SMS images of HeLa cells expressing (**b**) Halo-OMP25 and treated with HMSiR-CA or (**c**) treated with RhoB-TCO and HMSiR-Tz. The diffraction-limited image obtained from the RhoB channel is marked by the dashed white line in (c). Kymographs of both images, derived from the time-dependent signal along each brown line *vs.* time, are shown on the right side of each panel. Laser intensity: 4.4 kW/cm^2. Scale bar: 1 μm. The full 9 min movie is available as **Supplementary Movie 7.** (**d**) A plot of the fluorescent signal in both the SMS and diffraction-limited image as a function of position along the yellow line in (c). The signal from the SMS image is shown in teal; the signal from the diffraction-limited image is shown in black.

Figure 4 Long time-lapse, wide-field SMS imaging of the plasma membrane using the HIDE probes DiI-HMSiR and DiI-C6-HMSiR generated upon reaction of HMSiR-Tz with either DiI-TCO or DiI-C6-TCO. (**a**) Chemical structures of DiI-TCO and DiI-C6-TCO. (**b**) Super-resolution image of the plasma membrane visualized with the HIDE probe DiI-HMSiR. Laser intensity: 9.9 kW/cm^2. Scale bar: 1 μm. The image in the green box is magnified for clarity to illustrate the line profile quantified in (**c**). The image in the pink box is viewed at 5 time points in (d). (**c**) A plot of the fluorescent signal in both the SMS and diffraction-limited image as a function of position along white line within the green box in (b). The signal from the SMS image is shown in teal (fit to a Gaussian equation in orange with a FWHM of 36 nm); the signal from the diffraction-limited image is shown in black. Adjacent filopodia can be distinguished when separated by distances as small as 160 nm. (**d**) Time-lapse images of filopodia dynamics over the course of 96 s, with notable changes highlighted by yellow arrows. Scale bar: 1 μm. The diffraction-limited image is shown for comparison. The full 7 min movie is available as **Supplementary Movie 8.** (**e**) Comparison of the number of localizations per μm^2 as a function of time when cells were visualized using either DiI-HMSiR, DiI-C6-HMSiR, or Smo-HMSiR. Scale bar: 1 μm. (**f**) τ values calculated from a single exponential fit to the photobleaching curves in (e) (mean ± SD, n = 3-4 cells). The full 20 min movie obtained using DiI-C6-HMSiR is available as **Supplementary Movie 9.**
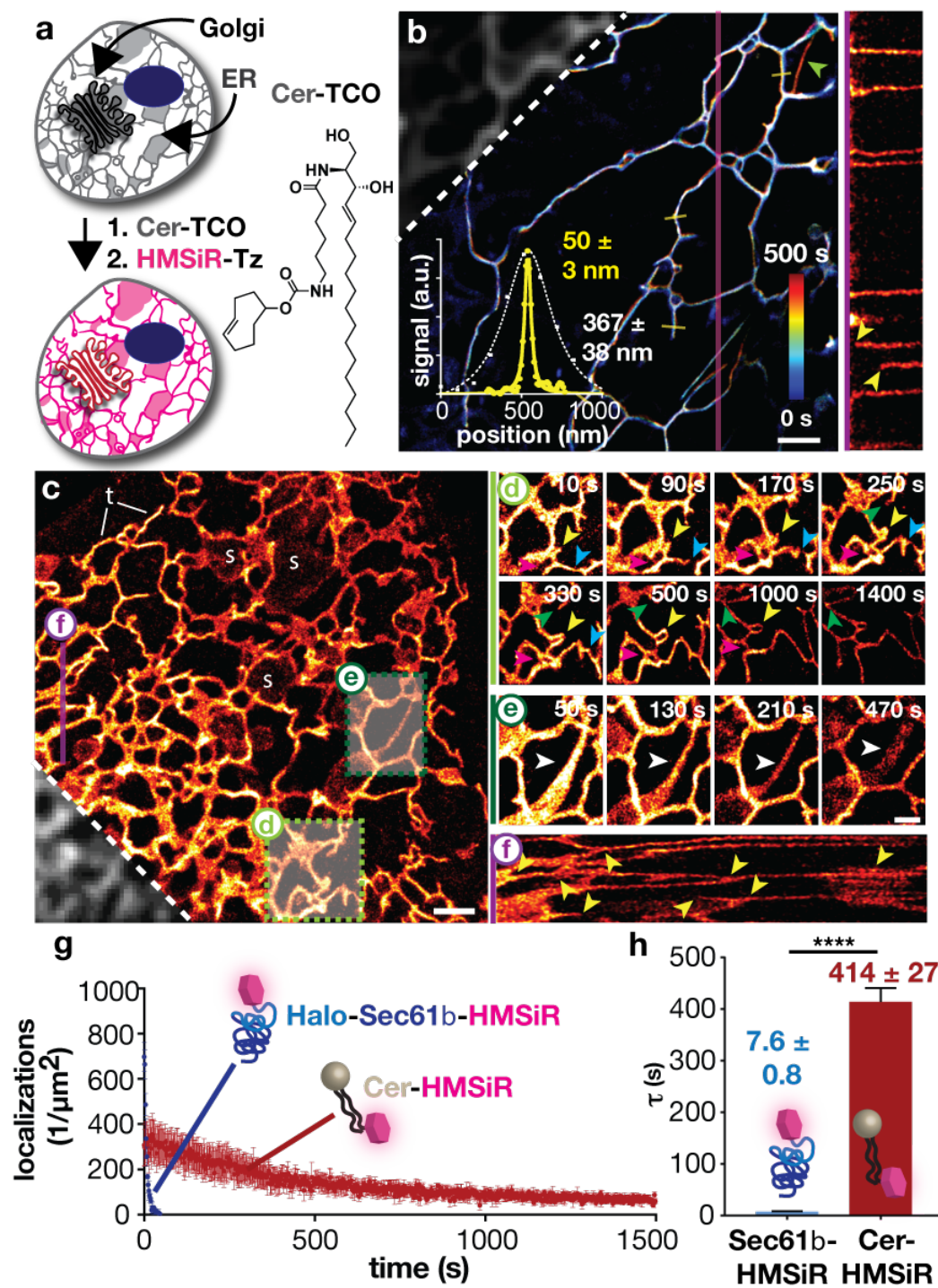
Figure 5 Two color SMS imaging of the ER in live cells. (**a**) SMS images of the ER in HeLa cells expressing the two ER markers KDELR-mEos3.2[37] (green) and Halo-Sec61β[11] and treated with HMSiR-CA (red). An enlarged view of the image within the yellow box is shown at right. (**b, top**) A plot of the average fluorescent signal as a function of position along the 6 profiles shown as pink lines.   These profiles are characterized by FWHM values (mean ± S.D., n = 6) of 53 ± 6 and 63 ± 12 nm in the green and red channels, respectively; (**b, bottom**) A plot of the intensity in both channels along the tubule boxed in blue. The red and green arrows identify regions where each probe is enriched. Laser intensities: 2.90 kW/cm^2 at 560 nm (KDELR-mEos3.2), 9.42 kW/cm^2 at 642 nm (Sec61β-HMSiR). (**c**) SMS images of COP1 vesicles and mitochondria in HeLa cells expressing the markers COPβ1-mEos3.2 (green) and Halo-OMP25 and treated with HMSiR-CA (red). An enlarged view of the image within the yellow box is shown beneath. Laser intensities: 3.08 kW/cm^2 at 560 nm (COPβ1-mEos3.2), 6.30 kW/cm^2 at 642 nm (OMP25-HMSiR). (**d**) SMS images of the COP1 vesicles and the Golgi in HeLa cells expressing the markers COPβ1-mEos3.2 (green) and treated with Cer-TCO and HMSiR-Tz at 20 °C (red). An enlarged view of the image within the yellow box is shown beneath. Laser intensities: 3.08 kW/cm^2 at 560 nm (COPβ1-mEos3.2), 6.30 kW/cm^2 at 642 nm (Cer-HMSiR). (**e**) SMS images of COP1 vesicles and the Golgi and ER in HeLa cells expressing the marker COPβ1-mEos3.2 (green) and treated with Cer-TCO and HMSiR-Tz at 37 °C (red). An enlarged view of the image within the yellow box is shown beneath. Laser intensities: 3.08 kW/cm^2 at 560 nm (COPβ1-mEos3.2), 6.30 kW/cm^2 at 642 nm (Cer-HMSiR). All scale bars: 1 µm.
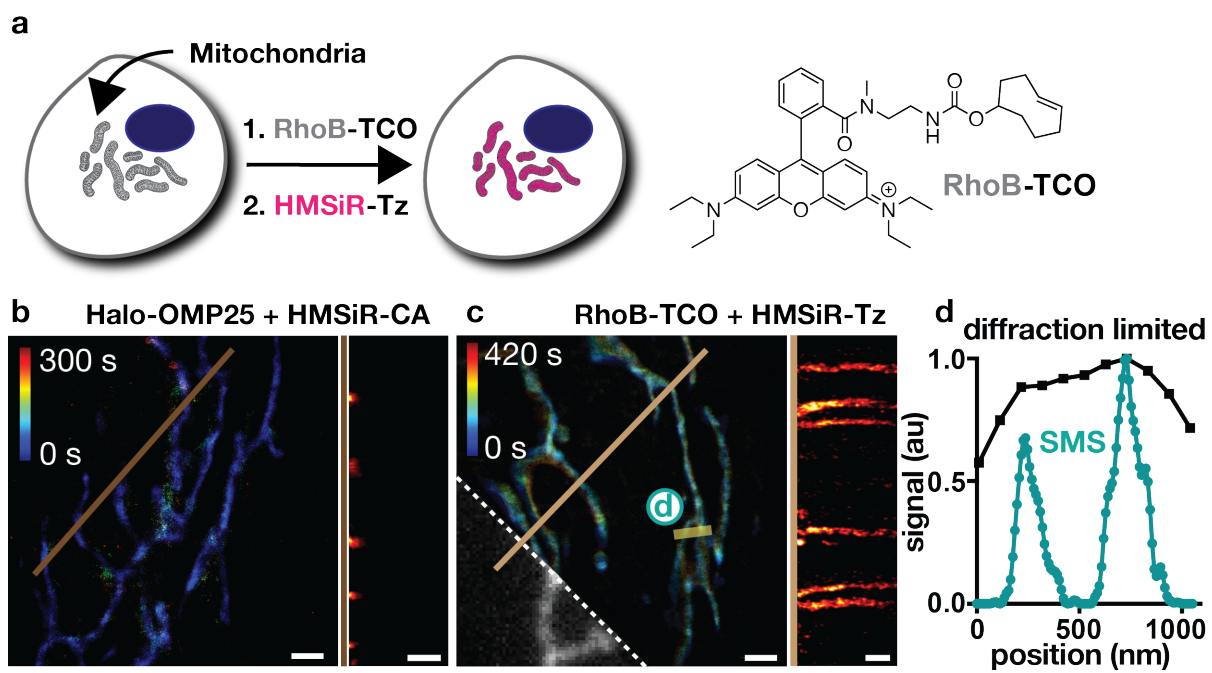
Figure 6 3D long time-lapse, wide-field imaging the ER with the HIDE probe Cer-HMSiR. (**a**) Depth-colored snapshot of a 15 min movie of the ER in HeLa cells treated with Cer-TCO and HMSiR-Tz. Laser intensity 9.7 kW/cm^2. The full movie is available as **Supplementary Movie 11,** rendered for 3D glasses as **Supplementary Movie 12.**   (**b**) Perspective view of the snapshot shown in (**a**). (**c**) Top view of the magenta cube shown in (**b**) highlighting tubules t_1-t_4. (**d**) Front view of the magenta cube shown in (**b**) highlighting tubules t_1-t_4 and their connections c_1-c_3. (**e**) Cartoon representation of the three dimensional arrangement of tubules shown in the magenta cube. A multi-perspective 3D zoom-in view of this region is shown in **Supplementary Movie 10.** (**f**) 3D time-lapse images of HeLa cells treated with Cer-TCO and HMSiR-Tz; the region in the orange box is shown at 4 different time points. The full movie is available as **Supplementary Movie 13.** (**g**) Snapshot of the nucleus-proximal region of the ER of a HeLa cell labeled with Cer-TCO and HMSiR-Tz. (**h**) *y,z*-cross section of the red box in (g). (**i**) Line profile of the area in the brown box in (**h**) with FWHM values of 167 and 118 nm for the ER-derived channel and the ER structure associated with the nucleus. All images/movies were recorded at 9.7 kW/cm^2.

a Mitochondria
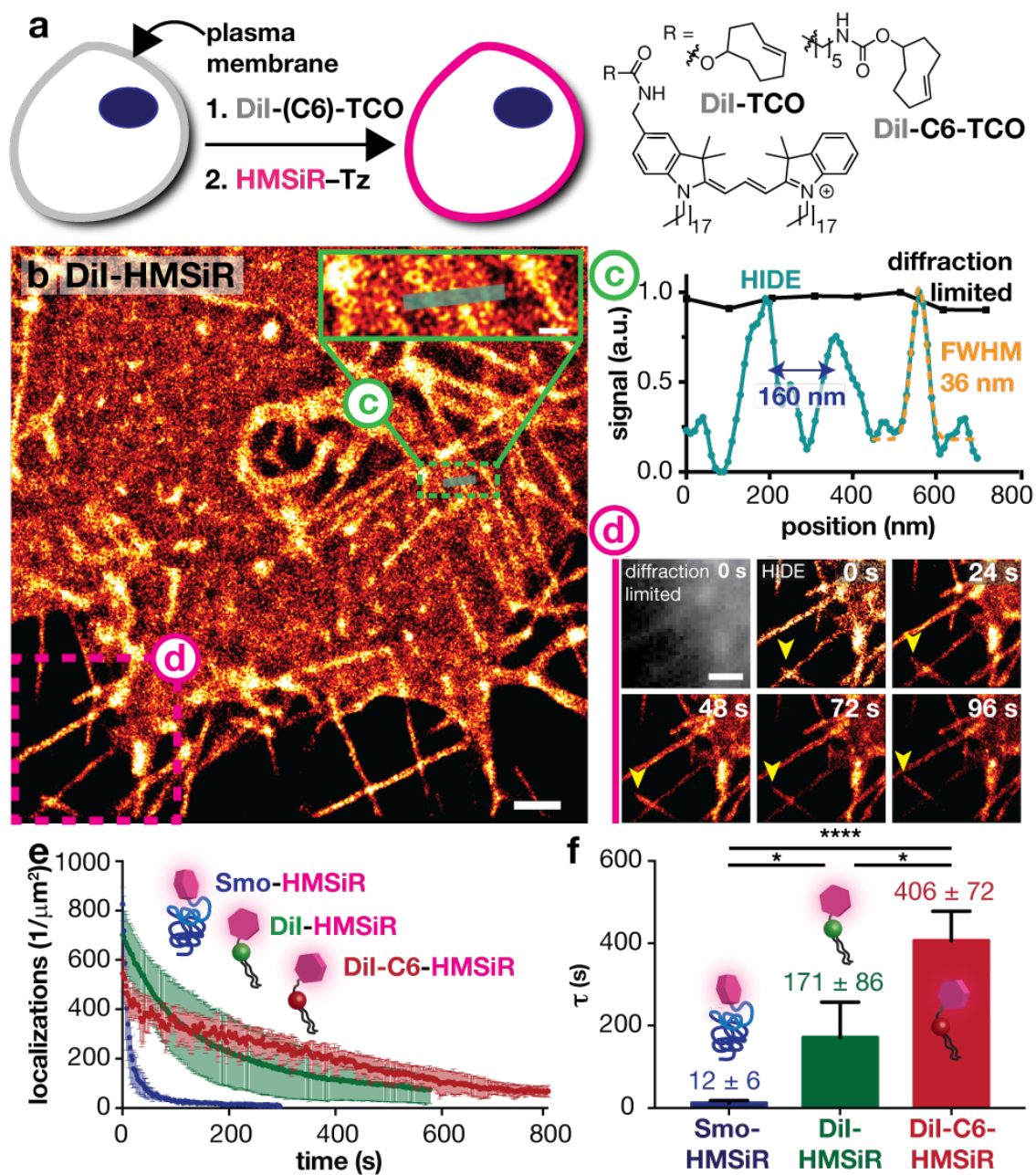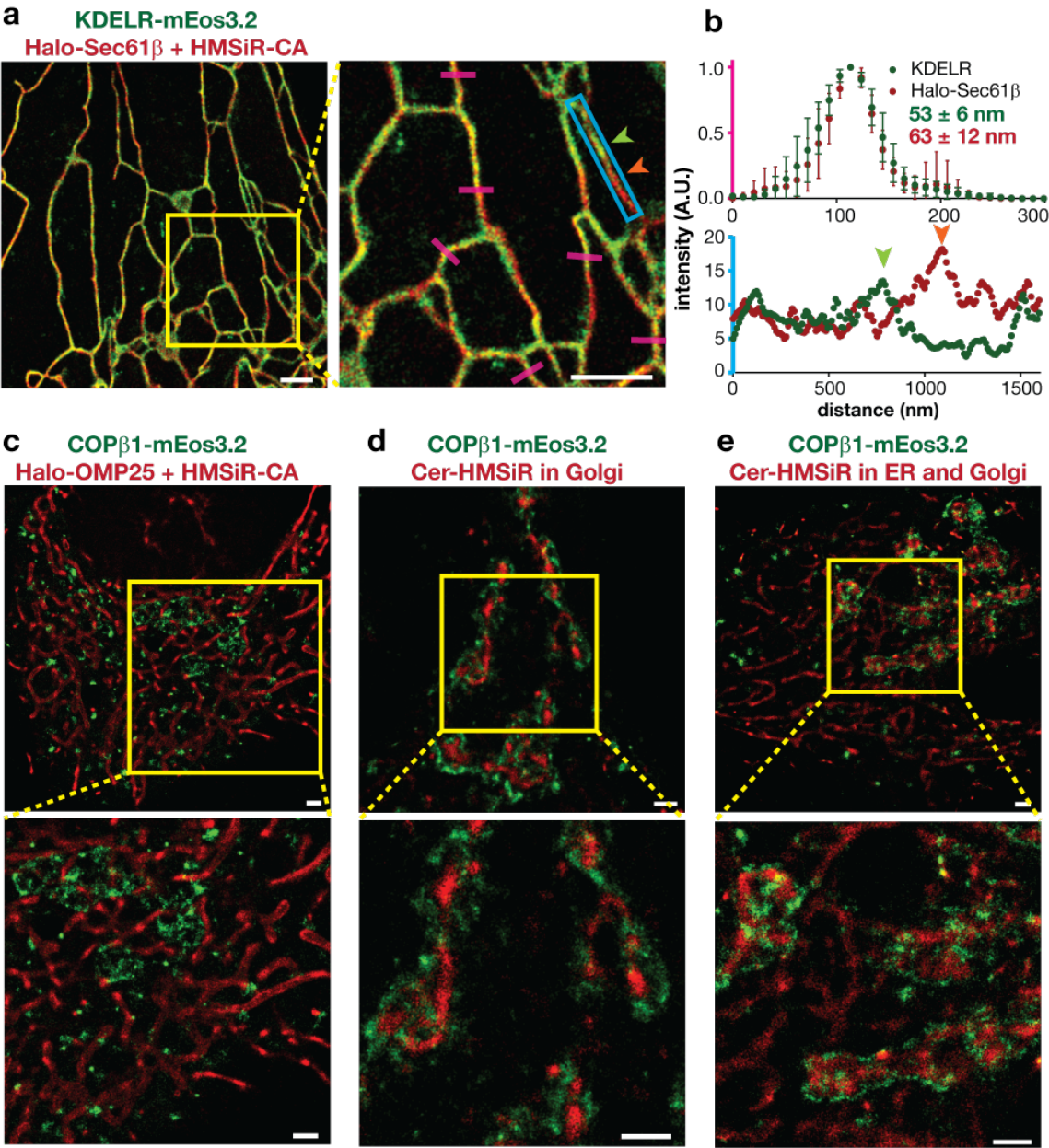1. RhoB-TCO
2. HMSiR-Tz
RhoB-TCO

b Halo-OMP25 + HMSiR-CA
300 s
0 s

c RhoB-TCO + HMSiR-Tz
420 s
0 s

d diffraction limited
SMS

Takakura et al. Fig. 5

a KDELR-mEos3.2
Halo-Sec61β + HMSiR-CA

b
intensity (A.U.)
KDELR
Halo-Sec61β
53 ± 6 nm
63 ± 12 nm
distance (nm)

c COPβ1-mEos3.2
Halo-OMP25 + HMSiR-CA

d COPβ1-mEos3.2
Cer-HMSiR in Golgi

e COPβ1-mEos3.2
Cer-HMSiR in ER and Golgi